

Phenomenological level density model with hybrid parameterization of deformed and spherical state densities

Naoya Furutachi* †, Futoshi Minato and Osamu Iwamoto

Nuclear Data Center, Japan Atomic Energy Agency, Tokai-mura, Naka-gun, Ibaraki 319-1195, Japan

A phenomenological level density model that has different level density parameter sets for the state densities of the deformed and the spherical states, and the optimization of the parameters using experimental data of the average s-wave neutron resonance spacing are presented. The transition to the spherical state from the deformed one is described using the parameters derived from a microscopic nuclear structure calculation. The nuclear reaction calculation has been performed by the statistical model using the present level density. Resulting cross sections for various reactions with the spherical, deformed and transitional target nuclei show a fair agreement with the experimental data, which indicates the effectiveness of the present model. The role of the rotational collective enhancement in the calculations of those cross sections is also discussed.

Keywords: nuclear level density; nuclear data; statistical model; neutron spectrum

*Corresponding author. Email: naoya.furutachi@riken.jp

†Present address: RIKEN Nishina center, 2-1 Hirosawa, Wako, Saitama 351-0198, Japan

1. Introduction

The level density (LD) is a key ingredient in the nuclear reaction calculation using the statistical model. The accuracy of the calculated nuclear reaction observables for various reaction channels relies on the LD, and therefore a number of theoretical works employing phenomenological[1, 2, 3, 4] or microscopic models[5, 6, 7, 8, 9, 10, 11] have been devoted to achieve a reliable LD. While the microscopic models are basically free from adjustable parameters and suitable to predict LDs of nuclei away from the stability line, the phenomenological models that have analytical formula and adjustable parameters are still useful to calculate LDs of nuclei around the stability line for the practical applications. Generally, the reliability of the phenomenological models is ensured with the experimental information of excitation energies and spin-parity of the low-lying discrete states, and the average of the s-wave neutron resonance spacing D_0 .

One of the key effects for LD is the enhancement due to the collective nuclear excitations. It is theoretically indicated that the collective rotational excitation brings an extremely large enhancement on the LD, which amounts to 10~100 magnitude at the neutron threshold energy of stable nuclei[12, 4]. In spite of its huge effect, the phenomenological LD models without the explicit treatment of the collective enhancement have been successfully applied to the nuclear reaction calculations for practical uses, for example, the LD model of Gilbert and Cameron[1] without the collective enhancement[2] has been mainly used in the statistical model calculation of the neutron induced reaction under 20 MeV for the nuclear data evaluation of Japanese Evaluated Nuclear Data Library (JENDL)[13]. The reason why such a LD model does not cause serious problems in nuclear reaction calculations is conjectured that the collective enhancement is effectively taken into account in LD parameters, if they are optimized using the experimental D_0 [2, 3].

Actually, such an effective LD model works well for the optimization of the asymptotic level density parameter to reproduce D_0 . Koning et al.[3] have derived the global LD

parameter systematics for the several LD models with and without explicit treatment of the collective enhancement. As for the Fermi-Gas based models, both the collective and the effective LDs have a similar precision for the reproduction of D_0 to each other.

It is noted that, besides the phenomenological models discussed here, the importance of the explicit treatment of the collective excitation is rather obvious in the microscopic LD calculations using Hartree-Fock plus Bardeen-Cooper-Schrieffer (HF+BCS) theory with the partition function method[6,7], and Hartree-Fock-Bogiliubov (HFB) theory with the combinatorial method[8,9,10,11]. All these studies treated the collective excitation explicitly, and found a fair agreement between the calculated D_0 and the experiments. These results indicate that if the intrinsic state densities are calculated without the parametrization, the collective enhancements are naturally required.

The role of the explicit treatment of the collective enhancement in phenomenological LD models can be discussed from nuclear reaction calculations. Koning et al.[3] have applied the the effective and the collective LD models to systematic calculations of the nuclear reactions. The calculated cross sections are systematically different between them for various reaction channels. The difference is expected to be more significant in a nuclear reaction at a higher incident energy, because the asymptotic behaviors of LD models with and without the collective enhancement are quite different. Actually, the important role of the collective enhancement in the cross section calculation for the projectile fragmentation with a relativistic incident energy have been reported[14].

However, there remains problems in the description of the collective enhancement in phenomenological models. One is the fading of the collective enhancement as a function of the excitation energy. Although there are some theoretical investigations about the fading of the collective enhancement[15], it is difficult to confirm their validity directly from the experiments, because it is expected that there is a finite mean deformation even with the excitation energy of several tens of MeV[15] for well-deformed nuclei. In addition

to that, it is also difficult to describe the rotational collective enhancement for nuclei in the transitional region, because the interaction between the single-particle states and the collective states plays a significant role in this case.

Our aim in this paper is to present a reliable LD necessary for the precise calculation of nuclear reaction observables using the statistical model. For this purpose, we propose a new phenomenological model based on the LD model of Gilbert and Cameron[1], in which the state densities of the deformed and spherical states have different level density parameters. The optimization of the parameters are performed by fitting the experimental D_0 with distinction between deformed and spherical nuclei. The LDs of the deformed and the spherical states are smoothly connected by the damping function, in analogy with the way used in the microscopic calculations based on HF+BCS and HFB[6,7,8,9,10,11]. The fading of the rotational collective enhancement is effectively described in this way. Since there is no direct experimental information about the fading of the rotational collectivity, we utilized the microscopic nuclear structure calculation to determine the parameters in the damping function. By the composition of the deformed and spherical states, the transitional state may be also effectively taken into account.

In this study, much attention is paid on the effectiveness of the present LD model for the actual nuclear reaction calculations. We use CCONE code[16] to calculate the cross sections, which are compared with the experimental data. At the same time, we investigate the role of the explicit treatment of the collective enhancement in nuclear reactions.

This paper is organized as follows. In Sec. 2, the formulation of the present LD model, the optimization procedure of the level density parameters, and the microscopic nuclear structure calculation are presented. In Sec. 3, first the characteristics of the present LD is discussed, then the results of the nuclear reaction calculations are shown. Sec. 4 summarizes this work.

2. Formulation

We present a new phenomenological LD model that is described with the LDs of the deformed and the spherical states connected by the damping function in a similar way to that used in the microscopic calculations based on HF+BCS and HFB[6, 7, 8, 9, 10, 11]. By optimizing the level density parameters for the deformed and the spherical states separately, reliable LDs for both deformed and spherical nuclei are expected to be achieved. We call the present model as the hybrid model to distinguish from the existing phenomenological collective models.

2.1. hybrid level density model

The LD of the present hybrid model ρ_h is described with the LD of the spherical state ρ_{sph} , and that of the deformed state ρ_{def} ,

$$\rho_h(U, J) = \begin{cases} (1 - f_{\text{dam}}(E_x))\rho_{\text{sph}}(U - E_{\text{def}}, J) + f_{\text{dam}}(E_x)\rho_{\text{def}}(U, J) & (E_{\text{def}} \geq E_{\text{cut}}) \\ \rho_{\text{sph}}(U, J) & (E_{\text{def}} < E_{\text{cut}}), \end{cases} \quad (1)$$

which are smoothly connected by the damping function f_{dam} ,

$$f_{\text{dam}}(E_x) = \frac{1}{1 + e^{(E_x - E_{\text{ts}})/d_e}}, \quad d_e = CE_{\text{ts}}. \quad (2)$$

Here E_x , U and J are the excitation energy, the pairing corrected excitation energy and the total angular momentum of the nucleus. In this formulation, the fading of the rotational collectivity is phenomenologically expressed by the transition from ρ_{def} to ρ_{sph} . Since experimental information about the fading of the rotational collectivity is limited, we derived the parameters E_{def} and E_{ts} that control this transition from the microscopic nuclear structure calculation, which is explained in Sec. 2.2.. The parameter E_{def} is defined as the energy difference between the deformed ground state and the minimum energy of the spherical state. If E_{def} is smaller than E_{cut} , the level density is approximated with ρ_{sph} . The parameter E_{cut} is arbitrary fixed at 0.3 MeV. The parameter E_{ts} is the central energy of the transition, which is estimated utilizing information of the deformation at a

finite temperature. The width parameter d_e of the damping function is phenomenologically determined supposing a linear dependence on E_{ts} with the adjustable parameter C . The detailed discussion for the parameter C is given in Sec. 2.4.. The pairing corrected effective excitation energy U is,

$$\begin{aligned}
 U &= E_x - 2\Delta && \text{for even-even nuclei} \\
 &= E_x - \Delta && \text{for odd nuclei} \\
 &= E_x && \text{for odd-odd nuclei} \\
 \Delta &= 11/\sqrt{A}. && (3)
 \end{aligned}$$

The functions ρ_{sph} and ρ_{def} are described by the phenomenological Fermi-gas model with the level density parameters a_s and a_d , respectively,

$$\begin{aligned}
 \rho_{\text{sph}}(U, J) &= R_s(U, J) \frac{\omega_s(U)}{\sqrt{2\pi\sigma_s}}, \\
 \rho_{\text{def}}(U, J) &= K_{\text{rot}} R_d(U, J) \frac{\omega_d(U)}{\sqrt{2\pi\sigma_d}}, && (4)
 \end{aligned}$$

$$\omega_{s,d}(U) = \frac{\sqrt{\pi} \exp(2\sqrt{a_{s,d}U})}{12 a_{s,d}^{1/4} U^{5/4}}, && (5)$$

here $R_{s,d}(U, J)$ are the spin distribution functions, and ω_s and ω_d are the state densities for ρ_{sph} and ρ_{def} , respectively. The rotational collective enhancement is explicitly treated in ρ_{def} by applying the enhancement factor K_{rot} . Contrary to the rotational collective enhancement, vibrational one is not explicitly treated in our formulation. We expect that it is implicitly taken into account through the optimization of the level density parameters.

The level density parameters $a_{s,d}$ are given as,

$$a_{s,d}(U) = a_{s,d}(\ast) \left[1 + \frac{E_{\text{sh}}}{U} (1 - e^{-\gamma U}) \right], && (6)$$

here $a_{s,d}(\ast)$ are the asymptotic level density parameters described by the systematics,

$$a_{s,d}(\ast) = \alpha_{s,d} A (1 - \beta_{s,d} A^{-1/3}). && (7)$$

The parameters $\alpha_{s,d}$, $\beta_{s,d}$, and γ are optimized using the experimental D_0 , as explained

in the next subsection. The shell correction energy E_{sh} is defined as,

$$E_{\text{sh}} = M_{\text{exp}} - M_{\text{LDM}}, \quad (8)$$

here the mass formula of Myers and Swiatecki are[17] used for M_{LDM} . It is noted that the pairing energy systematics in Eq. 3 is consistent with the one used in the calculation of M_{LDM} .

The spin distribution function $R_{\text{s,d}}(U, J)$ are

$$R_{\text{s,d}}(U, J) = \frac{2J+1}{2\sigma_{\text{s,d}}^2} \exp \left[-\frac{(J+1/2)^2}{2\sigma_{\text{s,d}}^2} \right], \quad (9)$$

here we employ the shell-corrected spin dispersion function of Mughabghab and Dunford[18],

$$\sigma_{\text{s,d}}^2 = I_0 \frac{\sqrt{a_{\text{s,d}} U}}{a_{\text{s,d}} (*)}, \quad (10)$$

$$I_0 = \frac{\frac{2}{5} m_0 R^2 A}{(\hbar c)^2} = 0.01389 A^{5/3} \text{ MeV}^{-1}. \quad (11)$$

The rotational enhancement factor K_{rot} is written as,

$$K_{\text{rot}} = \sigma_{\perp}^2, \quad (12)$$

$$\sigma_{\perp}^2 = I_0 \left(1 + \frac{\beta_2}{3} \right) \sqrt{\frac{U}{a_{\text{d}}}}. \quad (13)$$

In the present model, the composite formula of Gilbert and Cameron[1] is used. The low excitation energy region below the matching energy E_{m} is described by the constant temperature part $\rho_{\text{CT}}(E_x, J)$,

$$\begin{aligned} \rho_{\text{GC}}(E_x, J) &= R_{\text{h}}(U, J) \rho_{\text{CT}}(E_x) & (E_x < E_{\text{m}}), \\ \rho_{\text{GC}}(E_x, J) &= \rho_{\text{h}}(E_x, J) & (E_x \geq E_{\text{m}}). \end{aligned} \quad (14)$$

Here the spin distribution function $R_{\text{h}}(U, J)$ is calculated by,

$$R_{\text{h}}(U, J) = \rho_{\text{h}}(U, J) / \rho_{\text{h}}^{\text{tot}}(U), \quad \rho_{\text{h}}^{\text{tot}}(U) = \sum_J \rho_{\text{h}}(U, J), \quad (15)$$

where ρ_{CT} is given by,

$$\rho_{\text{CT}}(E_x) = \frac{1}{T} \exp\left(\frac{E_x - E_0}{T}\right), \quad (16)$$

here E_0 and T are determined from the usual matching condition[1]. The pairing corrected matching energy $U_m = E_x - 2\Delta$ (even-even), $E_x - \Delta$ (odd), E_x (odd-odd) are given by the simple systematics,

$$U_m^{\text{sys}} = pA^x, \quad (17)$$

where the mass dependence of the systematics is introduced to fit the U_m determined to reproduce the experimental discrete level numbers. The optimization procedures for the parameters p, x are explained later.

If the pairing corrected energy U is smaller than 0, the spin distribution function $R_h(U, J)$ cannot be calculated by Eq. 15. To avoid this, we simply extrapolate $R_h(U, J)$ at $U = 1$ MeV to $U < 1$ MeV region.

Finally, we assume the equal parity distribution function, namely

$$\rho_{\text{GC}}(E_x, J, \Pi) = \frac{1}{2} \rho_{\text{GC}}(E_x, J). \quad (18)$$

2.2. *microscopic nuclear structure calculation*

In the present model, results of the microscopic nuclear structure calculation is utilized to determine the transition from the deformed LD to the spherical LD. We performed the nuclear structure calculation using FTHFB theory, and derived the most probable deformation β_2 as a function of the excitation energy. The excitation energy is calculated using the energy expectation values of the system with the temperature T ,

$$E_x = E(T) - E(T = 0). \quad (19)$$

The calculation was executed with HFBTHO code[19], where the energy density functional of SkM*[20] was used. We employed the surface-volume mixed type pairing in-

teraction with the pairing cutoff energy $\epsilon_{cut} = 60$ MeV. The neutron and the proton pairing strengths are determined to reproduce the experimental pairing gap derived from the three-point mass difference for ^{120}Sn and ^{138}Ba , which have the proton and neutron closed shells of $Z=50$ and $N=82$, respectively.

[Figure 1 about here.]

In Fig. 1, the most probable β_2 as a function of the excitation energy is shown. Basically the most probable β_2 decreases as the excitation energy increases, but its behavior is different for each nucleus. For example, while ^{80}Se has a larger β_2 than ^{133}Cs at the ground state, the most probable β_2 decreases more rapidly and becomes 0 at slightly smaller energy than ^{133}Cs . We define E_{ts} as the energy where the most probable β_2 value becomes 0, because it can be a indicative of the loosing of the rotational collective enhancement, and derived it systematically for stable nuclei. The obtained E_{ts} are shown in Fig. 2. We found that the most of the deformed nuclei of $A < 150$ have E_{ts} of $10 \sim 20$ MeV. This means that the disappearance of the deformation may affect nuclear reactions with incident beam energy even below 20 MeV, which are often calculated using the statistical model for nuclear data libraries. For deformed nuclei in $A > 150$ region, the most of them have large E_{ts} which are well above the maximum excitation energy of the compound nucleus formed with 20 MeV incident nucleon.

In the present model, we suppose that the spherical states appear in the excited state after exhausting the deformation energy that is defined as the energy difference between the spherical and the deformed ground state energies,

$$E_{\text{def}} = E_{\text{const.}}^{\beta_2=0}(T=0) - E(T=0). \quad (20)$$

This energy is subtracted from the excitation energy of $\rho_{\text{sph}}(U, J)$, as described by Eq. 1.

[Figure 2 about here.]

2.3. *effective and collective level density models*

For comparison, we also derive the LDs using the effective and collective models. The effective model is defined with $\rho_{\text{sph}}(U, J)$ used in the present hybrid model,

$$\rho_{\text{eff}}(U, J) = \rho_{\text{sph}}(U, J), \quad (21)$$

and the collective model is defined as,

$$\begin{aligned} \rho_{\text{col}}(U, J) &= \max([K_{\text{rot}} - 1] f(E_x) + 1, 1) R_d(U, J) \frac{\omega_d(U)}{\sqrt{2\pi}\sigma_d}, \\ f_{\text{dam}}(E_x) &= \frac{1}{1 + e^{(E_x - E_{\text{col}})/d_{\text{col}}}}, \end{aligned} \quad (22)$$

here E_{col} and d_{col} are fixed at 30 MeV and 5 MeV, which are the values used by Koning et al.[3]. For both $\rho_{\text{eff}}(U, J)$ and $\rho_{\text{col}}(U, J)$, the constant temperature part are combined in the same way as the hybrid model.

2.4. *optimization procedure*

Basically the optimization of the systematics for the asymptotic level density parameter was performed in a similar way to Mengoni and Nakajima[2]. It is noted that the constant temperature model is not used in the optimization procedure for the asymptotic level density parameters for simplicity.

The parameters to be optimized using the experimental values of the average s-wave neutron resonance spacing D_0 are $\alpha_{\text{s,d}}$, $\beta_{\text{s,d}}$ and γ in Eq. 6 and 7. We determine $\alpha_{\text{s,d}}$ and $\beta_{\text{s,d}}$ to minimize χ_a^2 defined as,

$$\chi_a^2 = \sum_i \frac{(a_i^{\text{local}}(*) - a_i^{\text{sys}}(*)^2)}{a_i^{\text{sys}}(*)}, \quad (23)$$

here $a_i^{\text{local}}(*)$ is the asymptotic level density parameter derived to reproduce the experimental D_0 for each nucleus, and $a_i^{\text{sys}}(*)$ is that calculated by Eq. 7. Here i is the index to specify nucleus. The experimental D_0 values for 300 nuclei are taken from RIPL-3

database[21]. Once $\alpha_{s,d}$ and $\beta_{s,d}$ are determined, we calculate $f_{\text{rms}}^{D_0}$ defined as,

$$f_{\text{rms}}^{D_0} = \exp \left[\frac{1}{N_{\text{max}}} \sum_{i=1}^{N_{\text{max}}} \ln^2 \frac{D_0(\text{cal.})}{D_0(\text{exp.})} \right]^{1/2}, \quad (24)$$

where $D_0(\text{cal.})$ are calculated using $a^{\text{sys}}(*)$. The above procedure is performed using various γ parameters, and finally the set of $\alpha_{s,d}$, $\beta_{s,d}$ and γ that gives the minimum value of $f_{\text{rms}}^{D_0}$ is determined. Obtained parameters and $f_{\text{rms}}^{D_0}$ are listed in Table 1.

[Table 1 about here.]

In more detail, the procedure to determine $\alpha_{s,d}$ and $\beta_{s,d}$ is divided into two steps. First we determine α_s and β_s . For the spherical nuclei that have the condition $E_{\text{def}} < E_{\text{cut}}$, D_0 is calculated only from ρ_{sph} . Therefore, a_s^{local} can be determined independently from a_d . In the left top panel of Fig. 3, $a_s^{\text{local}}(*)$ of 108 nuclei with $E_{\text{def}} < E_{\text{cut}}$ are shown by the open squares, and $a_s^{\text{sys}}(*)$ determined by minimizing χ_a^2 with these $a_s^{\text{local}}(*)$ is shown by the solid line. Secondly, α_d and β_d are determined. To calculate D_0 for nuclei with $E_{\text{def}} \geq E_{\text{cut}}$, both $a_s(*)$ and $a_d(*)$ are necessary. We calculate $a_s(*)$ using $a_s^{\text{sys}}(*)$ determined from the above procedure, and derive $a_d^{\text{local}}(*)$ to reproduce the experimental D_0 for 182 nuclei with $E_{\text{def}} \geq E_{\text{cut}}$. The obtained $a_d^{\text{local}}(*)$ and $a_d^{\text{sys}}(*)$ are shown by the open circles and the broken line in the left top panel of Fig. 3, respectively. It is clearly seen that smaller $a_d(*)$ values are required compared to $a_s(*)$, which indicates that the spherical and the deformed intrinsic states should have different state densities. It is noted that we excluded 10 nuclei with small deformations of $E_{\text{cut}} < E_{\text{def}} < 0.5$ MeV, in which ρ_h is dominated by ρ_{sph} . In such a case, extremely large or small values of $a_d^{\text{local}}(*)$ appears to reproduce D_0 , and it is unfavorable for the optimization of $a_d^{\text{sys}}(*)$.

[Figure 3 about here.]

The hybrid model has an additional parameter C that adjusts the width parameter d_e of f_{dam} . While we use the theoretical values for the central energy E_{ts} of f_{dam} , the width parameter d_e that express a smoothness of the transition is quite phenomenological. Therefore, we investigated the dependence on C in the calculation of D_0 . In Fig. 4, $f_{\text{rms}}^{D_0}$ as

a function of C is shown. While it is clear that a small C is not preferable, C dependence of $f_{\text{rms}}^{D_0}$ is so moderate in larger C region, which means that D_0 cannot be an strong constraint on C . Basically we used $C = 0.35$ that is smaller than the optimal value for D_0 that is around 0.70, since a better agreement between calculations and experimental data of the nuclear reaction cross sections was obtained with $C = 0.35$, in the case of (n,2n) reactions for Se isotopes discussed in the next section.

[Figure 4 about here.]

We also optimized the parameters for the effective and the collective LD models. For these models, all the experimental D_0 values for 300 nuclei are used for the optimization of $a^{\text{sys}}(*)$. The obtained $a^{\text{local}}(*)$ and $a^{\text{sys}}(*)$ for the effective and the collective models are shown in the middle and the bottom panels of Fig. 3, respectively, and the parameters in $a^{\text{sys}}(*)$ and $f_{\text{rms}}^{D_0}$ calculated using the optimized $a^{\text{sys}}(*)$ are listed in Table 1. Although significantly different parameters are required for $a_s^{\text{sys}}(*)$ and $a_d^{\text{sys}}(*)$, the resulting $f_{\text{rms}}^{D_0}$ are similar among the effective, collective and hybrid models. As already mentioned in the introduction, the essentiality of the explicit treatment of the collective enhancement is hardly seen in the calculation of D_0 , if the phenomenological LD models optimized using the experimental D_0 are used.

Finally, the parameters in the constant temperature part of LD are optimized. The parameters to be optimized are p and x in Eq. 17 to calculate U_m^{sys} . They are determined to minimize χ^2 calculated as same as Eq. 23 using U_m^{sys} and U_m^{local} , and U_m^{local} is determined to minimize

$$f_{\text{rms}}^{\text{lev}} = \exp \left[\frac{1}{N_{\text{max}}} \sum_{i=1}^{N_{\text{max}}} \ln^2 \frac{L_{E_i}(i)(\text{cal.})}{L_{E_i}(i)(\text{exp.})} \right]^{1/2}, \quad (25)$$

here $L_{E_i}(i)$ is the cumulative number of the discrete levels at the excitation energy E_i of the experimentally observed i -th level, and N_{max} is the number of levels to be compared. The experimental data of the discrete levels are taken from RIPL-3 database[21]. Since there may be discrete levels that have not been observed, the cumulative number of the

observed levels is expected to deviate from the reality with increase of the excitation energy. We assume that the deviation is small if the cumulative number of the observed levels is much smaller than the maximum number of the observed levels, and arbitrary take 70% of the maximum number as N_{\max} . Nuclei with more than 100 observed levels are used to determine the parameters of U_m^{sys} . In Fig. 5, the obtained U_m^{local} and U_m^{sys} are shown by the symbols and the solid line, respectively. It is seen that U_m^{local} are roughly reproduced by the mass dependence of U_m^{sys} , except for the values around $A \sim 200$. We take priority to achieve better precision for U_m in $A < 200$ region, which are relevant to the nuclear reaction calculations in the next section, and excluded U_m^{local} in $A > 200$ region from the fitting for this preference. In the final results presented in the next section, the optimized U_m^{sys} is used to calculate LD.

[Figure 5 about here.]

2.5. Nuclear reaction models

The nuclear reaction calculations have been executed using CCONE code[16]. The code composed of the optical model, two-component exciton model, distorted-wave Born approximation and Hauser-Feshbach statistical model. As for the optical model, the global optical potential parameters of Koning and Delaroche[22] was used. LDs of the hybrid, effective and collective models are adopted to Hauser-Feshbach statistical model in CCONE code by using the tabulated numerical data of RIPL-3 format[21].

3. results

3.1. Total level densities

Before showing the results of the nuclear reaction calculations, the characteristics of the hybrid model are discussed from the total LDs in comparison with the effective and collective models. In Fig. 6, the total LDs of ^{82}Se , ^{90}Zr , ^{169}Tm and ^{197}Au in wide excitation

energy range, and those magnified around the neutron threshold are shown in the left and right panels, respectively. The parameters relevant to the deformation that determine the characteristic of the present hybrid model are summarized in Table 2. As described by Eq. 1 and 2, the transition to ρ_{sph} from ρ_{def} is made by these parameters. Hereafter, we denote the LDs of the hybrid, effective and collective models as ρ_{h} , ρ_{eff} and ρ_{col} , respectively.

[Figure 6 about here.]

[Table 2 about here.]

First of all, for the spherical ^{90}Zr case, ρ_{h} is close to ρ_{eff} in the entire region, while ρ_{col} is significantly different from them, because there is the rotational collective enhancement even in the spherical nuclei with the fixed E_{col} of 30 MeV. In addition to that, because of the difference in the asymptotic level density parameters, the increase rate of ρ_{col} above 30 MeV is also different from ρ_{h} and ρ_{eff} . As for ^{169}Tm that has a developed deformation with $\beta_2 = 0.32$, ρ_{h} shows a similar behavior to ρ_{col} below about 30 MeV. They deviate from each other above 30 MeV, because the rotational collective enhancement fades in ρ_{col} around this energy, but does not in ρ_{h} . As for ^{82}Se that has a moderately developed deformation of $\beta_2 = 0.16$, the component of ρ_{def} in ρ_{h} is decreasing around $E_x \sim E_{\text{ts}}=7.5$ MeV. In $E_x > 20$ MeV, ρ_{h} comes closer to ρ_{eff} , because the component of ρ_{sph} dominates in this region. The difference between ρ_{h} and ρ_{eff} in the asymptotic region is characterized with the energy shift by E_{def} . ^{197}Au has a smaller β_2 of 0.13 but has a larger E_{def} than ^{82}Se . The increment of ρ_{h} significantly reduces around $E_x \sim E_{\text{ts}}=13$ MeV because the difference between the spherical LD shifted by E_{def} and the deformed LD is large. Above 20 MeV, the increase rate of ρ_{h} comes closer to ρ_{eff} , and deviates from ρ_{col} .

The LDs around the neutron threshold S_{n} are shown in the right panel of Fig. 6 as a function of $E_x - S_{\text{n}}$. Since the asymptotic LD parameters are optimized for all of ρ_{h} , ρ_{eff} and ρ_{def} using the experimental D_0 , they are close to each other at S_{n} . However, there is a difference in the increase rate of these LDs. In any case, ρ_{eff} has a larger increase rate

than ρ_{col} . Whether the increase rate of ρ_{h} is similar to that of ρ_{eff} or ρ_{col} is determined by the deformation. It is close to ρ_{eff} for the spherical ^{90}Zr , and ρ_{col} for the deformed ^{169}Tm and ^{197}Au . As for ^{82}Se , ρ_{h} has even smaller increase rate than ρ_{col} , because the component of ρ_{def} disappears just around S_{n} in this case. The increase rates of LDs around S_{n} have remarkable influences on the nuclear reaction calculations explained in the next subsection.

3.2. cross sections of (n,xn) and (p,xn) reactions

In this section, we test the effectiveness of LDs and also discuss the role of the rotational collective enhancement from the calculations of (n,xn) and (p,xn) reactions. The experimental data of the cross sections to be compared are taken from EXFOR[23] throughout this section.

To illustrate the role of the rotational collective enhancement, the (n,2n) and (n,3n) reactions with ^{90}Zr and ^{169}Tm targets that are spherical and deformed, respectively, are calculated. In addition to that, these nuclei have a plenty of (n,2n) experimental data to be compared. There are also (n,3n) experimental data for ^{169}Tm , but not for ^{90}Zr . Instead, the (n,3n) cross sections of ^{89}Y are calculated.

[Figure 7 about here.]

The results are shown in Fig. 7. As discussed in the previous subsection, ρ_{h} is similar to ρ_{eff} if the nucleus is spherical. Therefore, for the ^{90}Zr target, the (n,2n) cross sections calculated using ρ_{h} and ρ_{eff} are also similar, and they show good agreement with the experimental data. However, ρ_{col} is different from them even for the spherical ^{90}Zr , and cannot reproduce the experimental data. On the other hand, for the deformed ^{169}Tm target, the cross sections calculated with ρ_{h} are similar to those with ρ_{col} . Compared to the results with ρ_{eff} , the (n,2n) and (n,3n) cross sections are suppressed below 12 MeV and 25 MeV, respectively. The (n,3n) cross sections and the competing (n,2n) cross sections

above 15 MeV show good agreement with the experimental data. The difference in the calculated (n,2n) cross sections mainly come from the difference in the LDs of the target nuclei. In the (n,2n) reaction, first the $N + 1$ compound nucleus is formed, then it emits one neutron. If LD of the target nucleus has smaller increase rate around the neutron threshold, the emitted neutron brings more energy, which results in the increase of the competitive inelastic channel cross section, and decrease of the (n,2n) cross section. Later the difference in the neutron emission spectrum is discussed in detail.

[Figure 8 about here.]

Next we discuss the (n,2n) cross sections of Se isotopes shown in Fig. 8. If the target nucleus have a moderate deformation with E_{ts} close to S_n , the (n,2n) cross section calculated with ρ_h shows non negligible dependence on d_e , which is the width parameter of f_{dam} . ^{76}Se , ^{78}Se , ^{80}Se and ^{82}Se have $E_{ts}=12.2, 11.1, 10.1$ and 7.5 MeV, and $S_n=11.1, 10.5, 9.9$ and 9.3 MeV, respectively. The (n,2n) cross sections calculated with ρ_h and ρ_{col} show suppression from those with ρ_{eff} , as in the cases of ^{90}Zr and ^{169}Tm . As for the results with ρ_h , the degrees of the suppression depend on d_e . The results calculated using $C = 0.35$ and 0.70 are also compared in Fig. 8. If d_e is smaller, a decrease of the component of ρ_{def} in ρ_h is more rapid, which results in a smaller increase rate of LD. Therefore, the (n,2n) cross sections calculated with $C = 0.35$ tend to be suppressed compared to those with $C = 0.70$. While this effect is not significant for ^{76}Se , ^{78}Se and ^{80}Se cases, a noticeable difference is found for ^{82}Se , because ^{82}Se has E_{ts} just below S_n . In this case, the component of ρ_{def} becomes 0 just around S_n if $C = 0.35$ is used, which results in the significantly small increase rate of LD around S_n as shown in Fig. 6. As for ^{82}Se , the (n,2n) cross sections calculated with $C = 0.35$ are even smaller than those calculated with ρ_{col} .

These results indicate that the effect of the fading of the rotational collective enhancement around S_n can be seen in the (n,2n) cross section. The validity of this effect should be studied using as many experimental data as possible, but not so many (n,2n) exper-

imental data are available for nuclei that have E_{ts} close to S_n . Although the number of experiments is limited, Se isotopes have the systematic experimental data of Frehaut et al.[24]. The calculated results with $C = 0.35$ well agree with those data renormalized by the factor of 1.08, which is derived by Vonach et al.[25].

[Figure 9 about here.]

Another nucleus that has a plenty of experimental data and a moderate deformation is ^{197}Au . The calculated results of $^{197}\text{Au}(n,xn)$ cross sections are shown in Fig. 9. As discussed in the case of Se isotopes, the values of E_{ts} and S_n are important to understand the characteristics of the cross section calculated with ρ_h . E_{ts} is 13 MeV for ^{197}Au , while S_n and S_{2n} are 6.6 MeV and 15.0 MeV, respectively. Since E_{ts} is much larger than S_n and just below S_{2n} , both (n,2n) and (n,3n) cross sections show suppression from the results with ρ_{eff} below 14 MeV and 25 MeV, respectively. However, the (n,2n) and (n,3n) cross sections in $15 \text{ MeV} < E_n < 25 \text{ MeV}$, which are competing, show a disagreement with the experimental data. To investigate how the calculated cross sections depend on the degrees of the deformation, a modified ρ_h for ^{197}Au that has arbitrary chosen E_{ts} and E_{def} values of 8 MeV and 1 MeV is used to calculate the cross sections. The results are also shown in Fig. 9. Since $E_{ts} = 8 \text{ MeV}$ is well under S_{2n} , the suppression of the (n,3n) cross sections below 25 MeV is small. As a consequence, this results with the modified ρ_h show a better agreement with the experimental data in $15 \text{ MeV} < E_n < 25 \text{ MeV}$. As for the (n,4n) and (n,5n) cross sections, the results with both ρ_h of $E_{ts} = 8$ and 13 MeV are similar, because the incident energies are higher enough from E_{ts} for these channels, which means the complete disappearance of the component of ρ_{def} . The results with ρ_h significantly deviate from those with ρ_{col} in the higher incident energy region due to the difference of LDs in the asymptotic region. Several experimental data above 40 MeV support the results with ρ_h .

[Figure 10 about here.]

The suppression of (n,xn) cross sections calculated with ρ_h and ρ_{col} from those with ρ_{eff} is related to the difference in the evaporated neutron emission spectrum. To show this, the neutron emission spectrum of $^{nat}\text{Se}(n,xn)$, $^{nat}\text{Zr}(n,xn)$ and $^{197}\text{Au}(p,xn)$ reactions are calculated. The results are shown in the left panel of Fig. 10. The neutron emission spectrum of $^{nat}\text{Zr}(n,xn)$ reaction at 14.1 MeV calculated with ρ_{col} shows a noticeable enhancement around 5 MeV from those calculated with ρ_h and ρ_{eff} and a disagreement from the experimental data. It is consistent with the (n,2n) cross section calculated with ρ_{col} , which significantly deviates from the experimental data. Since ρ_{col} has a smaller increase rate at a excitation energy close to the incident nucleon energy, the evaporated neutrons from the compound nucleus tend to bring larger energies compared to the results with ρ_h and ρ_{eff} . In most cases, ρ_{col} has a smaller increase rate than ρ_{eff} , even for spherical nuclei. In $^{nat}\text{Se}(n,xn)$ case, the calculated result with ρ_h is similar to ρ_{col} , which show enhancement from the result with ρ_{eff} around 5 MeV.

In the right panel of Fig. 10, the neutron emission spectrum of $^{105,106,108,110}\text{Pd}(p,xn)$ reactions at $E_p = 26.1$ MeV are shown. For ^{105}Pd , ^{106}Pd , ^{108}Pd and ^{110}Pd , E_{ts} are calculated to be 10.0, 11.0, 14.3 18.0 and 20.3 MeV, respectively. While all of four Pd isotopes have moderate deformations around $\beta_2 \sim 0.2$, the difference in E_{ts} results in the significant difference in the evaporated neutron emission spectrum. Since ^{110}Pd has the largest E_{ts} that is close to E_p , the component of ρ_{def} in ρ_h affects the neutron emission from the compound nucleus. In this case, the neutron emission spectrum calculated with ρ_h is close to ρ_{col} , and deviates from that with ρ_{eff} . If E_{ts} is much smaller than E_p , the component of ρ_{def} has a small influence on the neutron emission from the compound nucleus. Therefore, the neutron emission spectrum calculated with ρ_h are similar to those with ρ_{eff} in $^{105}\text{Pd}(p,xn)$ and $^{106}\text{Pd}(p,xn)$ cases. This result illustrates the characteristic of the present LD model, and at the same time, the role of the collective enhancement in the evaporated neutron emission spectrum.

4. Summary

To construct a new phenomenological LD model for a better precision of the nuclear reaction calculation, and to investigate the role of the rotational collective enhancement in the nuclear reaction at the same time, we proposed the hybrid model in which the LDs of the deformed and the spherical states described by Fermi-Gas model are connected by the damping function. We optimized the asymptotic level density parameter systematics for the LDs of the deformed and the spherical states separately using the experimental D_0 of deformed and spherical nuclei, respectively. The information of the nuclear deformation derived from the FTHFB calculation was utilized. The obtained LD was introduced in the nuclear reaction calculation using the statistical model, and the cross sections of (n,xn) and (p,xn) reactions were discussed.

We found that the LD with the rotational collective enhancement tends to have a smaller increase rate compared to that with no explicit collective enhancement, which results in a higher energy neutron emission from the compound nucleus. The (n,xn) cross sections with incident neutron energies just above the threshold are suppressed because of this mechanism. In many cases, cross sections calculated with the transitional model were similar to those with the effective model and the collective model for the nuclear reactions for the spherical and the deformed targets, respectively. We showed the calculated examples for the spherical ^{90}Zr and the deformed ^{169}Tm targets, both of which agree with the experiments.

Depending on the incident nucleon energy and the degree of the deformation of the target nucleus, the cross sections have sensitivity to a certain energy range of LD where the component of the deformed state is decreasing. In $^{76,78,80,82}\text{Se}(n,2n)$ reactions, the decreasing component of the deformed state results in a good agreement between the calculated and the experimental cross sections. In $^{197}\text{Au}(n,xn)$ reactions, how cross sections depend on the degrees of the deformation was shown. These results indicate that a more

reliable prediction of deformations in excited states may lead to a more precise calculation of cross sections.

These results indicate that the present model is effective for precise calculations of nuclear reactions for both the spherical and deformed targets. Since the calculated cross section depends on the predicted deformations, a more precise cross section calculation can be achieved with a more reliable nuclear structure calculation in future. This model also can be a tool to investigate the fading of the rotational collective enhancement in nuclear excited states through the nuclear reaction calculation.

Acknowledgement

This work was funded by ImPACT Program of Council for Science, Technology and Innovation (Cabinet Office, Government of Japan).

References

- [1] Gilbert A, Cameron AGW. A composite nuclear level density formula with shell corrections. *Canadian J Phys.* 1965; 43:1446.
- [2] Mengoni A, Nakajima Y. Fermi-Gas Model Parametrization of Nuclear Level Density. *J Nucl Sci Technol.* 1994; 31:151-162.
- [3] Koning AJ, Hilaire S, Goriely S. Global and local level density models. *Nucl Phys A.* 2008; 810:13-76.
- [4] Ignatyuk AV, Istekov KK, Smirenkin GN. Role of collective effects in the systematics of nuclear level densities. *Sov J Nucl Phys.* 1979; 29:450.
- [5] Goriely S. A new nuclear level density formula including shell and pairing correction in the light of a microscopic model calculation. *Nucl Phys A.* 1996; 605:28-60.
- [6] Demetriou P, Goriely S. Microscopic nuclear level densities for practical applications. *Nucl Phys A.* 2001; 695:95-108.
- [7] Minato F. *J Nucl Sci Technol.* 2011; 48:984-992.

- [8] Hilaire S, Delaroche JP, Girod M. Combinatorial nuclear level densities based on the Gogny nucleon-nucleon effective interaction. *Eur Phys J A*. 2001; 12:169-184.
- [9] Hilaire S, Goriely S. Global microscopic nuclear level densities within the HFB plus combinatorial method for practical applications. *Nucl Phys A*. 2006; 779:63-81.
- [10] Goriely S, Hilaire S, Koning AJ. Improved microscopic nuclear level densities within the Hartree-Fock-Bogoliubov plus combinatorial method. *Phys Rev C*. 2008; 78:064307.
- [11] Hilaire S, Girod M, Goriely S, et al. Temperature-dependent combinatorial level densities with the D1M Gogny force. *Phys Rev C*. 2012; 86:064317.
- [12] Bour A, Mottelson BR. *Nuclear Structure Vols I and II*. New York: W. A. Benjamin Inc; 1969 and 1975.
- [13] Shibata K, Osamu I, Tsuneto N, et al. JENDL-4.0: A new library for nuclear science and engineering. *J Nucl Sci Technol*. 2011; 48:1.
- [14] Junghans AR, De jong M, Clerc H-G, et al. Projectile-fragment yields as a probe for the collective enhancement in the nuclear level density. *Nucl Phys A*. 1998; 629:635.
- [15] Hansen G, Jensen AS. Energy dependence of the rotational enhancement factor in the level density. *Nucl Phys*. 1983; 406:236.
- [16] Iwamoto O, Iwamoto N, Kunieda S, et al. The CCONE Code System and its Application to Nuclear Data Evaluation for Fission and Other Reactions. *Nucl Data Sheets*. 2016; 131:259-288.
- [17] Myers WD, Swiatecki WJ. *Nucl Phys*. 1966; 81:1.
- [18] Mughabghab SF, Dunford C. Nuclear Level Density and the Effective Nucleon Mass. *Phys Rev Lett*. 1998; 81:4083.
- [19] Stoitsov MV, Schunck N, Kortelainen M, et al. Axially deformed solution of the Skyrme-Hartree-Fock-Bogoliubov equations using the transformed harmonic oscillator basis (II) HF BTHO v2.00d: A new version of the program. *Comp Phys Communications*. 2013; 184:1592-1604.
- [20] Bartel J, Quentin P. Towards a better parametrisation of Skyrme-like effective forces: a critical study of the SkM force. *Nucl Phys A*. 1982; 386:79-100.

- [21] Capote R, Herman M, Obložinský, et al. RIPL - Reference Input Library for calculation of nuclear reactions and nuclear data evaluations. Nucl Data Sheets. 2009; 110:3107-3214.
- [22] Koning AJ, Delaroche JP. Local and global nucleon optical models from 1 keV to 200 MeV. Nucl. Phys. A. 2003; 713: 231-310.
- [23] Otuka N, Dupont E, Semkova V, et al. Towards a more complete and accurate experimental nuclear reaction data library (EXFOR): international collaboration between nuclear reaction data centres (NRDC). Nucl Data Sheets. 2014;120:272-276.
- [24] Frehaut J, Bertin A, Bois R, et al. Status of (n, 2n) cross section measurements at Bruyeres-le-Chatel. In: Bhat MR, Pearlstein S, editors. Proceedings of Symposium on Neutron Cross-sections from 10 to 50 MeV; 1980 May 12-14. Upton (NY): Brookhaven National Laboratory; 1980. p. 399-411.
- [25] Vonach H, Pavlik A, Strohmaier B. Accurate determination of (n, 2n) cross sections for heavy nuclei from neutron production spectra. Nucl Sci Eng. 1990;106:409-414.

Table 1 Parameters of the hybrid, effective and collective models, and calculated $f_{\text{rms}}^{D_0}$.

	hybrid	effective	collective
$f_{\text{rms}}^{D_0}$	1.66	1.74	1.66
α_s [MeV ⁻¹]	0.07110	0.06573	
α_d [MeV ⁻¹]	0.01291		0.03960
β_s	-3.608	-4.385	
β_d	-30.54		-5.708
γ [MeV ⁻¹]	0.072	0.073	0.098
p [MeV]	547	55	76
x	-1.10	-0.54	-0.74
E_{cut} [MeV]	0.30		
C	0.35		

Table 2 Calculated β_2 , E_{def} , E_{ts} and E_{m} of ^{82}Se , ^{90}Zr , ^{169}Tm and ^{197}Au . The experimental values of the one neutron separation energies are also shown.

	β_2	E_{def} (MeV)	E_{ts} (MeV)	E_{m}	S_{n} (MeV)
^{82}Se	0.16	1.31	7.5	6.7	9.3
^{90}Zr	0	0	0	6.2	12.0
^{169}Tm	0.32	19.2	90.5	2.8	8.0
^{197}Au	-0.13	3.1	13.0	2.4	6.9

Figure Captions

Figure 1 Most probable deformation β_2 as a function of the excitation energy calculated by FTHFB.

Figure 2 Parameter E_{ts} derived from FTHFB calculation.

Figure 3 Calculated $a^{(*)}$ (left panel) and D_0 (right panel) for the hybrid, effective and collective models. The $a^{(*)}$ determined to reproduce D_0 of each nucleus and calculated from the systematics are shown by the symbols and lines, respectively.

Figure 4 Dependence of $f_{rms}^{D_0}$ on the additional parameter C for the hybrid model.

Figure 5 Pairing corrected matching energy U_m^{local} obtained by minimizing f_{rms}^{lev} of each nucleus and U_m^{sys} calculated by Eq. 23 are shown by the symbols and the solid line, respectively. The red symbols are results for even-even nuclei, and the green ones for odd and odd-odd nuclei.

Figure 6 Total level densities of the hybrid (solid line), effective (dashed line) and collective (dotted line) LD models for ^{82}Se , ^{90}Zr , ^{169}Tm and ^{197}Au as a function of E_x (left panel) and $E_x - S_n$ (right panel).

Figure 7 Cross sections of (n,2n) reactions for ^{90}Zr and ^{169}Tm , and (n,3n) reactions for ^{89}Y and ^{169}Tm . Calculated results using ρ_h , ρ_{eff} and ρ_{col} are shown by solid, dashed and dotted lines, respectively. They are compared with the experimental data taken from EXFOR shown by symbols.

Figure 8 Cross sections of (n,2n) reactions for Se isotopes. Calculated results are same as in Fig. 7 except for the result using ρ_h with $C = 0.70$ shown by dash-dotted line. The experimental data of Frehaut et al. are renormalized by a factor of 1.08[25] (circle).

Figure 9 Cross sections of (n,xn) reactions for ^{197}Au . Calculated results are same as in Fig. 7 except for the result using ρ_h with $E_{ts} = 8$ MeV shown by dash-dotted line.

Figure 10 Neutron emission cross sections of (n,xn) and (p,xn) reactions. Calculated results are same as in Fig. 7. The experimental data are taken from EXFOR.

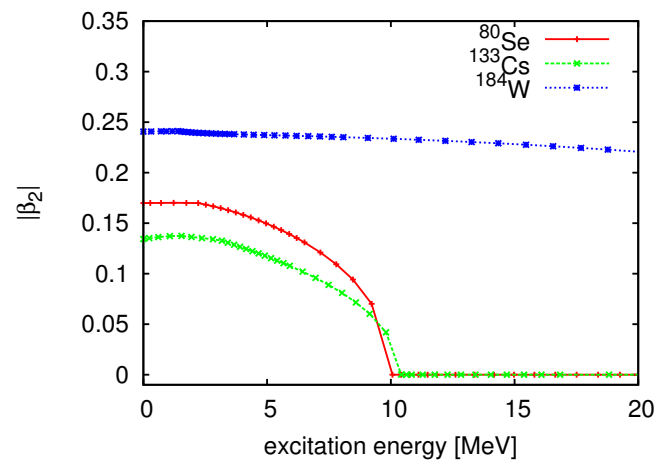


Figure 1 Most probable deformation β_2 as a function of the excitation energy calculated by FTHFB.

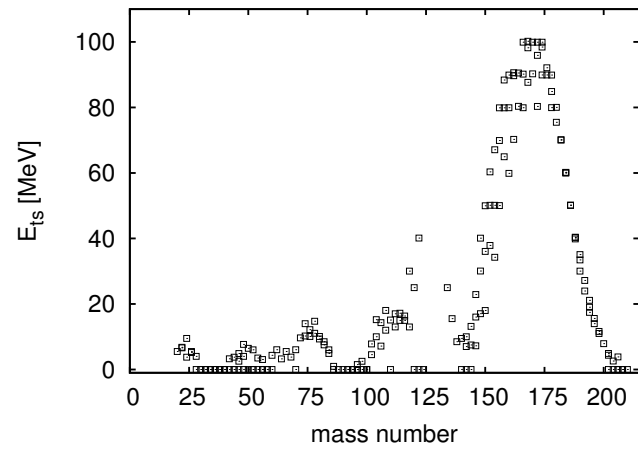


Figure 2 Parameter E_{ts} derived from FTHFB calculation.

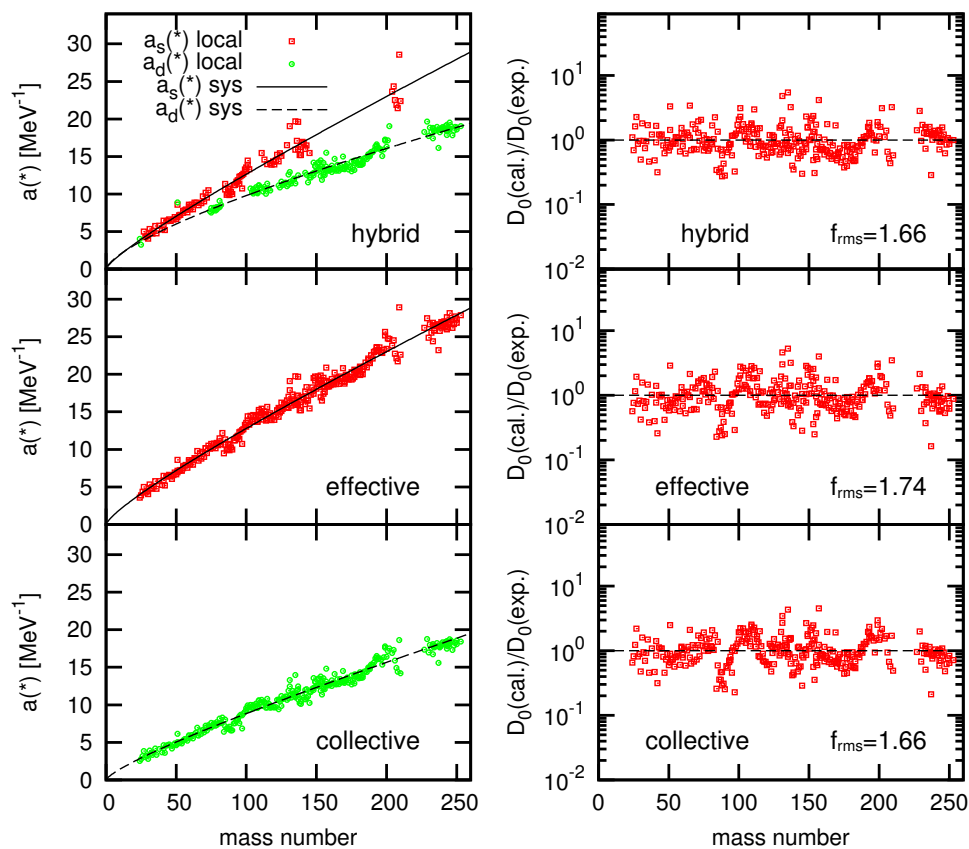


Figure 3 Calculated a^* (left panel) and D_0 (right panel) for the hybrid, effective and collective models.

The a^* determined to reproduce D_0 of each nucleus and calculated from the systematics are shown by the symbols and lines, respectively.

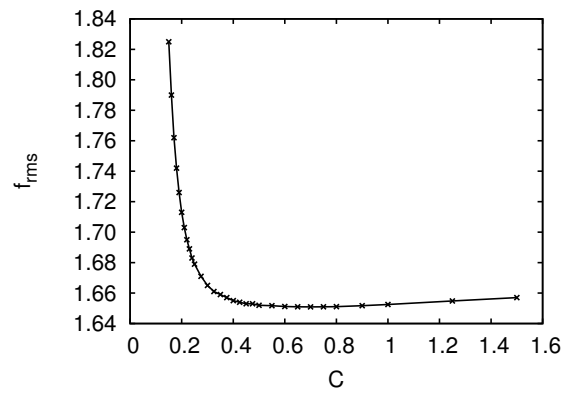


Figure 4 Dependence of $f_{rms}^{D_0}$ on the additional parameter C for the hybrid model.

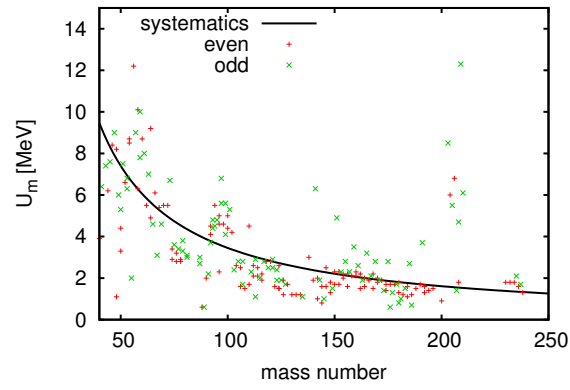


Figure 5 Pairing corrected matching energy U_m^{local} obtained by minimizing $f_{\text{rms}}^{\text{lev}}$ of each nucleus and U_m^{sys} calculated by Eq. 23 are shown by the symbols and the solid line, respectively. The red symbols are results for even-even nuclei, and the green ones for odd and odd-odd nuclei.

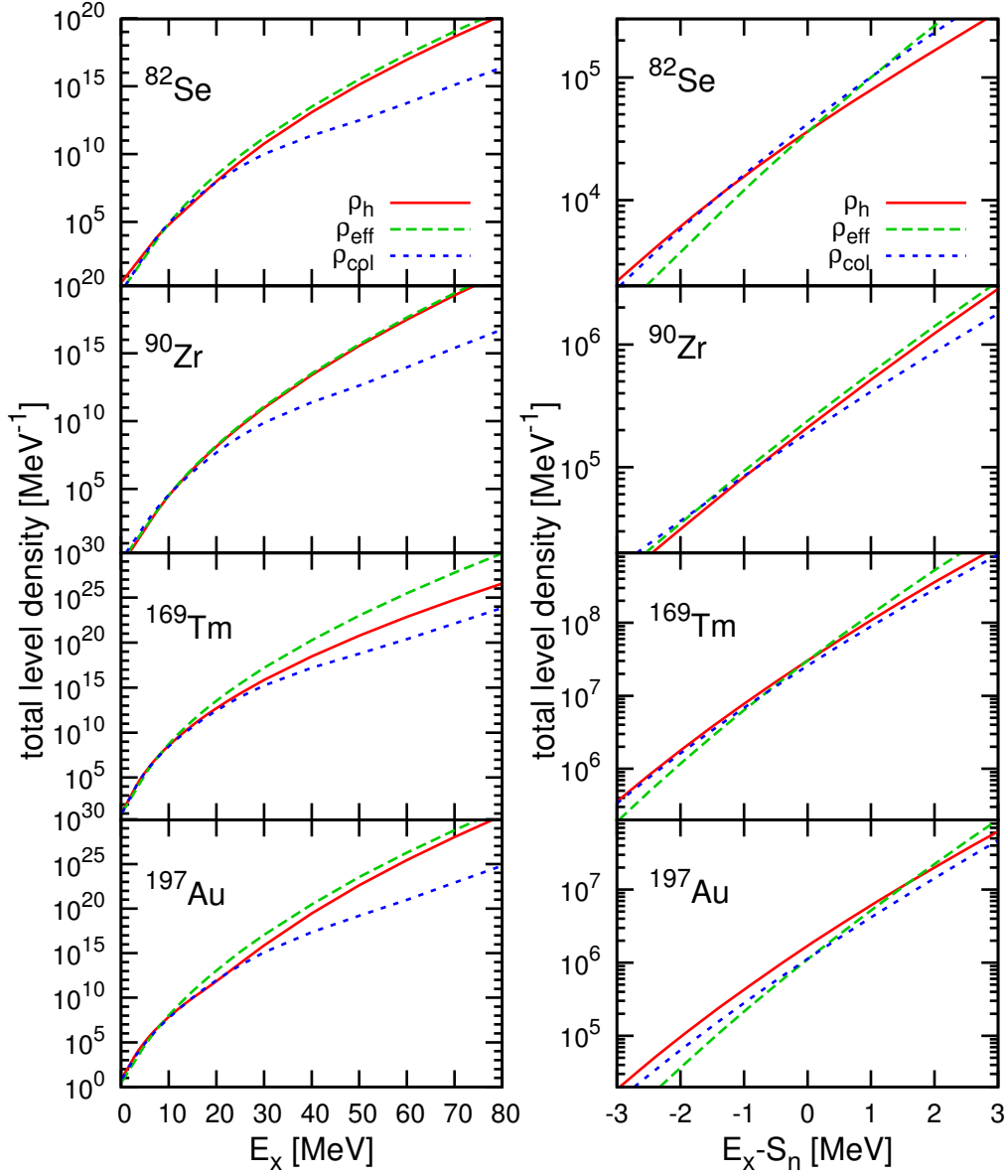


Figure 6 Total level densities of the hybrid (solid line), effective (dashed line) and collective (dotted line) LD models for ^{82}Se , ^{90}Zr , ^{169}Tm and ^{197}Au as a function of E_x (left panel) and $E_x - S_n$ (right panel).

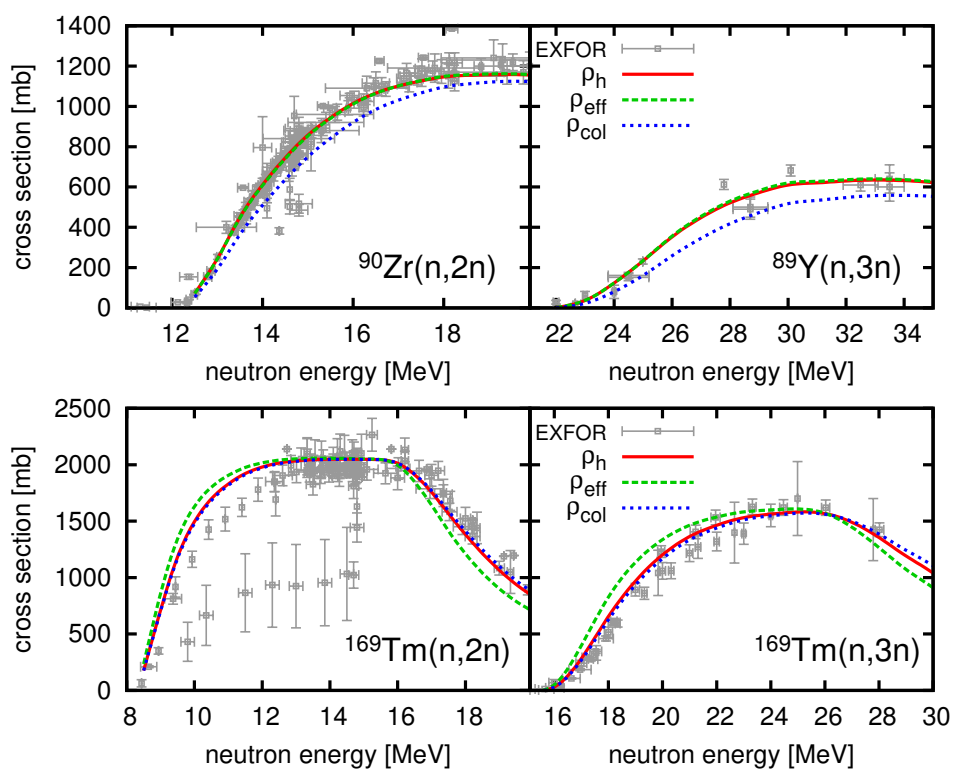


Figure 7 Cross sections of (n,2n) reactions for ^{90}Zr and ^{169}Tm , and (n,3n) reactions for ^{89}Y and ^{169}Tm .

Calculated results using ρ_h , ρ_{eff} and ρ_{col} are shown by solid, dashed and dotted lines, respectively.

They are compared with the experimental data taken from EXFOR shown by symbols.

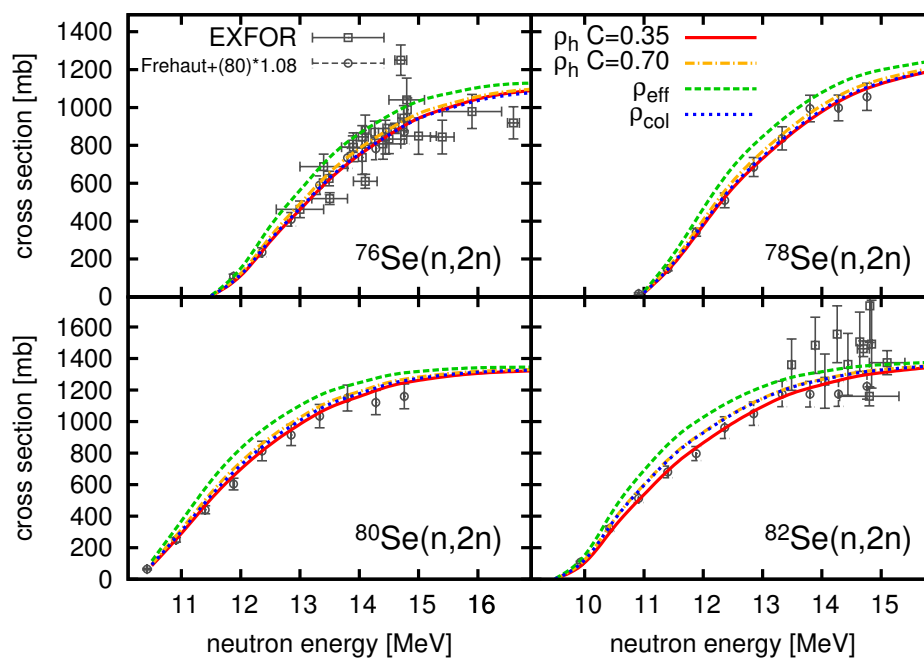


Figure 8 Cross sections of (n,2n) reactions for Se isotopes. Calculated results are same as in Fig. 7

except for the result using ρ_h with $C = 0.70$ shown by dash-dotted line. The experimental data of Frehaut et al. are renormalized by a factor of 1.08[25] (circle).

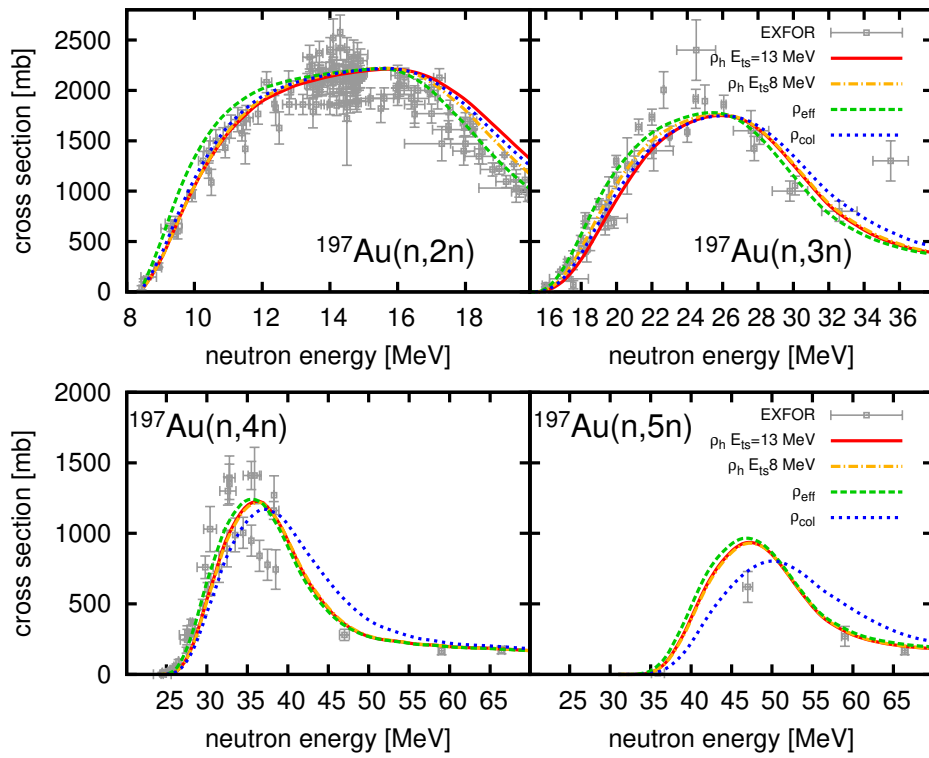


Figure 9 Cross sections of (n,xn) reactions for ^{197}Au . Calculated results are same as in Fig. 7 except for the result using ρ_h with $E_{ts} = 8$ MeV shown by dash-dotted line.

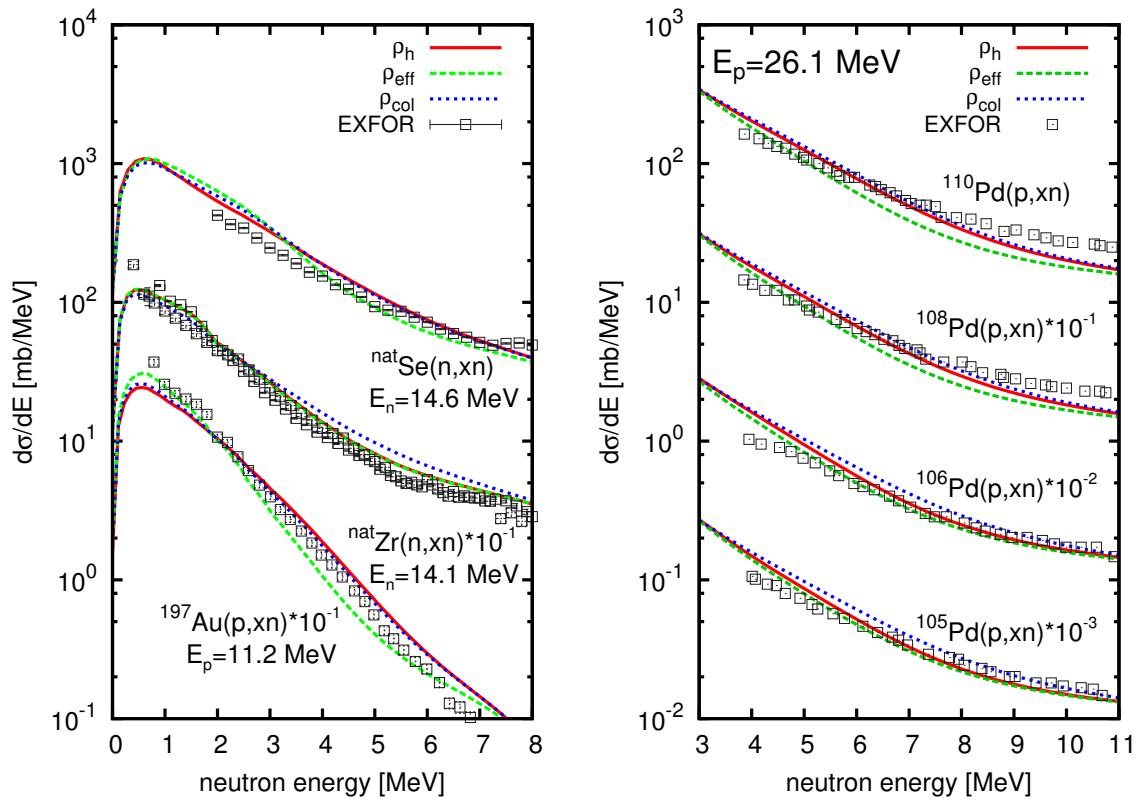


Figure 10 Neutron emission cross sections of (n,xn) and (p,xn) reactions. Calculated results are same as in Fig. 7. The experimental data are taken from EXFOR.